Oscillatory jets and instabilities in a rotating cylinder

Yohann Duguet, Julian F. Scott, Lionel Le Penven

Oscillatory jets and instabilities in a rotating cylinder

Yohann Duguet[a)]
School of Mathematics, University of Bristol, University Walk, BS8 1TW Bristol, United Kingdom

Julian F. Scott[a)] and Lionel Le Penven
Laboratoire de Mécanique des Fluides et d'Acoustique, UMR CNRS 5509—Ecole Centrale de Lyon, UCBL-Lyon 1, INSA-Lyon, 69134 Ecully Cedex, France

(Received 28 February 2006; accepted 1 September 2006; published online 11 October 2006)

The viscous flow inside a closed rotating cylinder of gas subject to periodic axial compression is investigated numerically. The numerical method is based on a spectral Galerkin expansion of the velocity field, assuming axisymmetry of the flow. If the forcing amplitude is weak and the angular forcing frequency is less than twice the rotation rate, inertial waves emanate from the corners, forming conical oscillatory jets which undergo reflections at the walls. Their thickness is $O(E^{1/3})$, or $O(E^{1/4})$ for particular forcing frequencies, where E is the Ekman number. For larger forcing amplitudes, the conical pattern breaks down. When the forcing frequency is resonant with a low-order inertial mode, the flow can undergo two types of parametric instabilities: a mode-triad resonance, and a subharmonic instability. The combination of both these mechanisms provides a possible route to quasiperiodicity of the flow. © *2006 American Institute of Physics*.
[DOI: 10.1063/1.2357973]

I. INTRODUCTION

Rotating flows dominated by the Coriolis force support inertial oscillations whose angular frequencies are bounded by twice the rotation rate.[1] Inertial wave propagation is known[2] to be dispersive and anisotropic, as shown by the inviscid dispersion relation $\omega=(2\boldsymbol{\Omega},\boldsymbol{k})/|\boldsymbol{k}|$, where $\boldsymbol{\Omega}$, ω, and $\boldsymbol{k}$ stand, respectively, for the angular velocity, dimensional angular frequency, and wave vector of a plane wave. Because of viscous damping, particularly in confined geometries, these oscillations naturally decay and need to be forced to remain observable on a long time scale. Several experiments have shown the existence of inertial modes inside a circular cylinder, when forced either directly[3–5] or by means of parametric resonance mechanisms,[6,7] the most studied being the elliptical instability.[8] Other studies have focused on inertial wave propagation inside a sphere[9–11] or a spherical shell[11–13] as a first step towards understanding of the geophysical dynamo in planetary cores.

If the forcing frequency ω_0 (nondimensionalized by the rotational frequency 2Ω) is smaller than unity, direct excitation of inertial waves is possible. According to their dispersion relation, the resulting inertial waves have group velocity $\boldsymbol{c}_g=(\boldsymbol{k}\times 2\boldsymbol{\Omega})\times\boldsymbol{k}/|\boldsymbol{k}|^3$, which is orientated at an angle $\phi=\arcsin\omega_0$ with the rotation axis. If such periodic forcing is applied locally in space and the rotation rate is large enough, inertial wave propagation manifests itself by the presence of thin conical shear zones inside the flow, whose orientation, determined by ϕ, depends on the value of ω_0 only.[3,14] These shear zones are the viscous counterpart of the conical characteristic surfaces arising from hyperbolicity of the inviscid Poincaré equation for the pressure[2] when $\omega_0<1$. Viscosity smooths out these singular surfaces, which become oscillatory jets/shear layers of fixed conical shape and can be interpreted in terms of the propagation of an inertial wave packet.[15] Such shear layers are thought to exist in natural systems such as atmospheres and planetary cores, where they are spawned by boundary layer eruptions at critical latitudes.[16] The steady case ($\omega_0=0$) corresponds to vertical shear layers (termed Stewartson layers), produced by differential rotation of the boundaries[17] and emanating from velocity discontinuities. These steady layers result from Ekman pumping and have an overall width of $O(E^{1/4})$, within which there is an inner layer of width $O(E^{1/3})$.[17] They are unstable once the Rossby number measuring nonlinear effects exceeds a certain threshold.[18,19] In the unsteady case, inertial wave propagation is oblique. Note that the jet width in McEwan's experiment[3] is $O(E^{1/3})$ before the flow breaks down ("collapses") to small scale disorder.

In this paper, we study the dynamics of oscillatory jets in a uniformly rotating flow inside a closed circular cylinder rotating about its axis at small E (see Fig. 1). The resulting solid-body rotation is perturbed by a weak periodic deformation, whose principal direction is that of the rotation axis. This periodic axial compression is produced by small sinusoidal oscillations of one of the end walls of the cylinder (henceforth referred to as the piston, and which is supposed to rotate at the same angular velocity as the cylinder itself). When the piston angular frequency ω_0 is less than twice the rotation rate, jets arise from the difference between the volume fluxes in the boundary layers which meet at the piston corner. Thus, in the interior of the cylinder, outside the boundary layers, the corner region acts as an oscillatory volumetric ring source.

Piston motion induces time variations of the cylinder height $h(t)$ as $h(t)=h_0(1+\epsilon\cos\omega_0 t)$, where h_0 is the mean aspect ratio, ω_0 is the angular frequency of the forcing, and ϵ

a)Author to whom correspondence should be addressed. Electronic mail: yohann.duguet@ec-lyon.fr

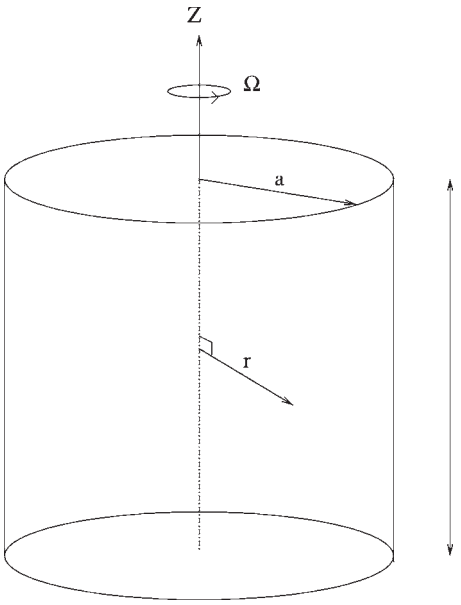

FIG. 1. Cylinder configuration and notation.

measures the forcing amplitude [note that, here and henceforth, space and time are nondimensionalized, respectively, by the cylinder radius a and rotation time $(2\Omega)^{-1}$]. The Ekman number is defined by $E=\bar{\nu}/2\Omega a^2$, where $\bar{\nu}$ is the time-averaged viscosity. The flow is supposed subject to the low Mach number regime and thermally isolated, thus all thermodynamic quantities are spatially homogenous, although time-dependent.[20]

The present configuration and its stability have been studied analytically,[20,21] experimentally[7] and numerically.[21,22] For small E and a large enough forcing amplitude, parametric instability occurs through coupling of inertial modes by axial piston motion. The asymptotic theory, based on small ϵ and small E, supposes that direct inertial-mode resonance, in which a low-order mode coincides with the forcing frequency to order $O(\epsilon)$, does not occur, leading to a viscous basic flow which differs only weakly from the inviscid one. This assumption is always valid when $\omega_0>1$, the case which has been the subject of the experimental and numerical work reported to date, but more detailed study of the case $\omega_0<1$ is needed, both to allow for the effects of direct resonance and because it leads to the formation of jets. This paper addresses these questions numerically for $\omega_0<1$ using an axisymmetric spectral code.

Throughout the paper, use is made of both local (propagating waves with wavelength small compared to the cylinder size) and global (inertial modes) descriptions when analyzing the numerical results. These approaches are complementary and, depending on the particular flow features considered, the one or the other may be more illuminating. The overall flow can always be exactly expressed as a sum over discrete inertial modes, but the modal description of small-scale flow structures requires many high-order modes and, in such cases, is cumbersome and not enlightening as it stands. For instance, the jets referred to above can be considered as a sum over many nearly resonant modes, but the wave description is clearer and can be derived asymptotically from the modal sum, but only following lengthy analysis. On the other hand, a modal approach is better in the case of, for instance, a single resonant mode or instabilities which result from interactions of a small number of modes.

The paper is organized as follows: Sec. II briefly describes the numerical method. In Sec. III A we show numerically that viscous jets are present in our configuration when $\omega_0<1$ and study their spatial structure for small forcing amplitudes. In Sec. III B we investigate the effect of larger forcing amplitude on the jets. Finally, in Sec. IV, we show that direct resonance of the basic flow can occur and affect the parametric instability mechanism.

II. NUMERICAL ALGORITHM

The numerical method used in these simulations has already been described in an earlier paper.[21] It is a spectral method based on the low Mach number approximation of the Navier-Stokes equations in the rotating frame. The time-dependent domain is first transformed into a fixed one, a cylinder of height h_0, by the coordinate transformation $X=x, Y=y, Z=z(h_0/h(t))$. The velocity field v is made divergence-free with respect to the new variables by defining $V_X=v_x, V_Y=v_y, V_Z=(h_0/h)(v_z-z\dot{h}/h)$. This change of velocity variables subtracts the flow, $v_x=v_y=0, v_z=z\dot{h}/h$, induced by piston motion in the absence of viscosity. The resulting field satisfies boundary conditions, arising from no-slip, which are singular at the corners, leading to discontinuities of the velocity field $\boldsymbol{V}$. In order to improve numerical convergence, $\boldsymbol{V}$ is split into two parts: (i) a sum of modified axisymmetric divergence-free Chebyshev polynomials weighed by time-dependent spectral amplitudes and (ii) an axisymmetric singular field, constructed analytically, which contains all the velocity singularities and mimics the Stokes flow near the corners. The governing equations are then projected onto the basis functions to yield a dynamical system for the spectral amplitudes, which is stepped forward in time from given initial conditions. For the parameter range of this study, numerical convergence requires 32 spectral functions in every direction and 200 time steps per piston period.

III. VISCOUS STRUCTURE OF THE BASIC FLOW

A. Small forcing amplitudes

Throughout this paper the cylinder aspect ratio is $h_0=4$. For all values of $\omega_0<1$, thin shear zones are visible in the velocity plots at small forcing amplitudes (see Fig. 2). Note that, in this figure, as in all subsequent velocity plots, the velocity field shown is $\boldsymbol{V}$, rather than $\boldsymbol{v}$. This removes the inviscid flow, making the flow structures, such as jets, stand out more clearly. When ϵ is very small compared to unity (here $\epsilon=10^{-3}$), the shear zones are conical, emanate from the piston corners, and propagate through the cylinder with reflections at the boundaries. The shear-zone flow oscillates in time with the same frequency as the piston, and will subsequently be referred to as "jets." The cones make a constant angle with the rotation axis, which can be determined to a precision which is limited by the finite jet width. For the case

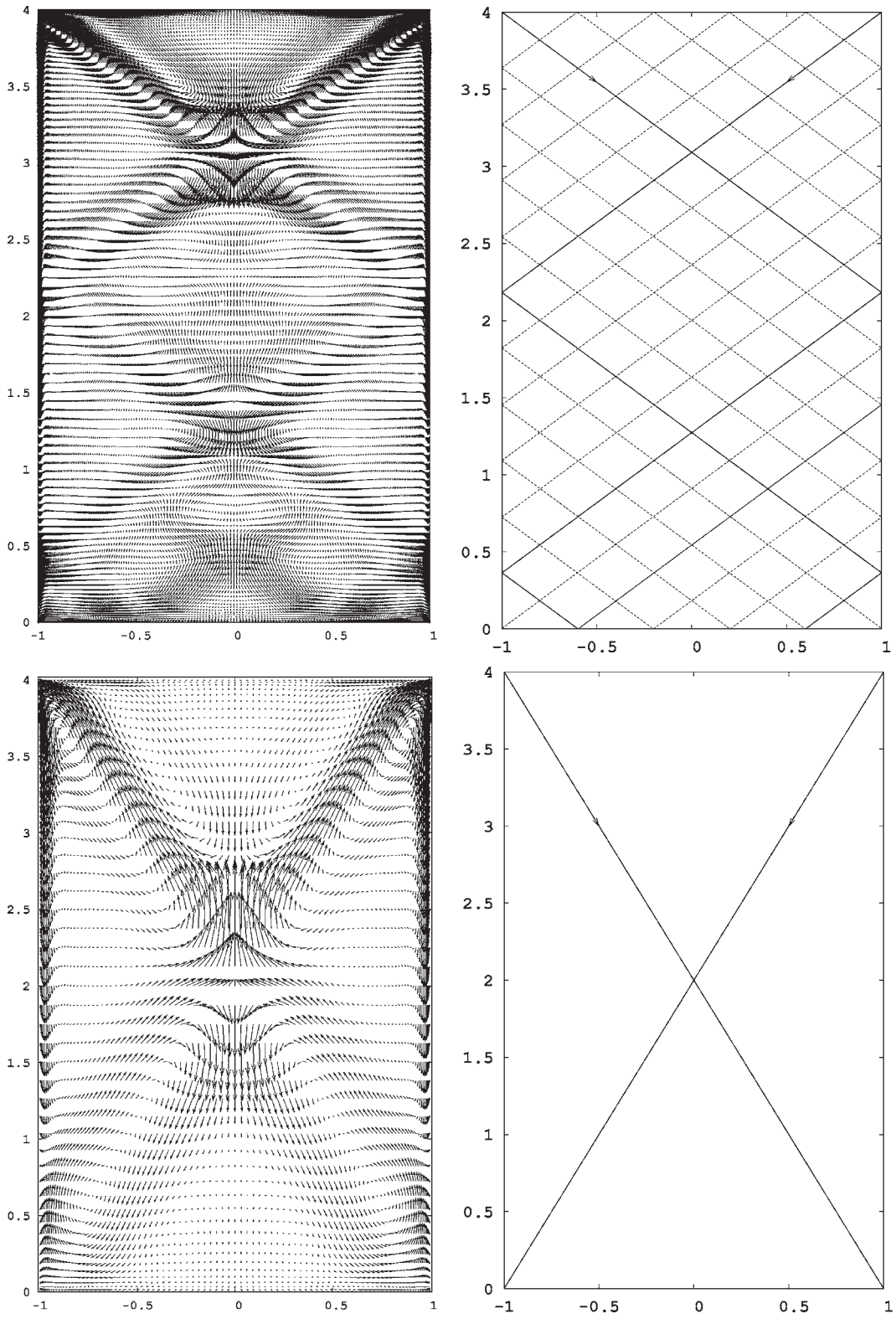

FIG. 2. Left-hand figures: velocity field $\boldsymbol{V}$ in a plane through the cylinder axis [$h_0=4$, $\epsilon=10^{-3}$, $E=5\times10^{-5}$, $\omega_0 t=0$ and $\omega_0=0.74$ (top), $\omega_0=0.4472$ (bottom)]. Right-hand figures: corresponding inviscid inertial-wave cones.

$\omega_0=0.74$ shown in Fig. 2 (top), the jets focus on the axis at $Z=3.1\pm0.1$, forming an angle of $48^\circ\pm3^\circ$. This agrees well with the inviscid theoretical angle $\phi=\arcsin\omega_0=47.7^\circ$, the angle between the rotation axis and the group velocity of inertial waves of angular frequency ω_0.

Two distinct cases occur, depending on the forcing frequency ω_0; the first when characteristics form a cyclic pattern and return after a finite number of reflections, the second when they do not. Note that angles are preserved by inertial-wave reflection since the walls of a cylinder rotating about its own axis are either parallel or orthogonal to the rotation axis. This allows simple geometrical rules for the description

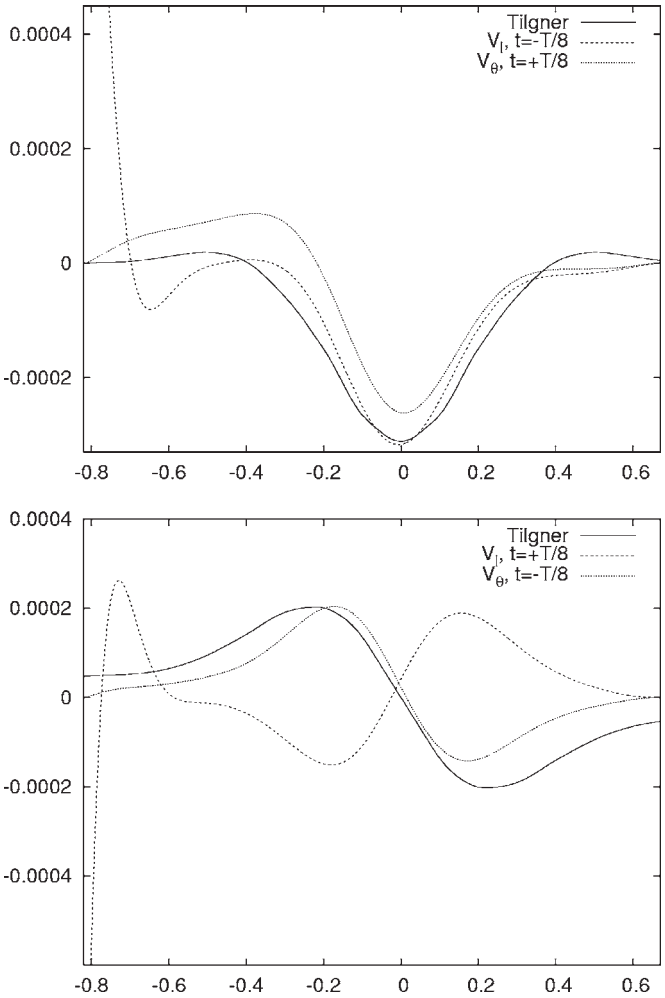

FIG. 3. Jet velocity profiles ($\epsilon=10^{-3}$, $E=5\times10^{-5}$, $\omega_0=0.74$) taken in a plane through the cylinder axis, along a line perpendicular to the direction of inviscid propagation at distance $R=0.74$ from the piston corner. V_θ is the azimuthal component of $\boldsymbol{V}$ (perpendicular to the given plane through the cylinder axis) and V_l its longitudinal component (in the plane and direction of inviscid propagation). Comparison with the analytical solution in an unbounded domain by Tilgner (Ref. 15).

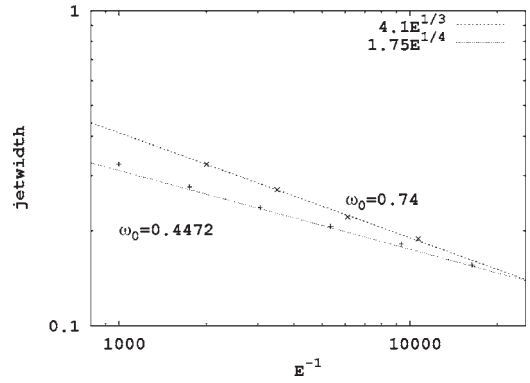

FIG. 4. Jet width as a function of E for $\epsilon=10^{-3}$, $\omega_0=0.4472$, and 0.74.

of the characteristic paths. In the absence of viscosity, the first case corresponds theoretically to $h_0 \tan \phi$ being a rational number. However, viscous dissipation prevents the characteristics from achieving a large number of reflections. This is illustrated by Fig. 2 (top left), which corresponds to the inviscid pattern shown in Fig. 2 (top right), but only the first few reflections are apparent. On the other hand, in Fig. 2 (bottom left), the jet structures undergo reflection at the opposite corner and return to the source corners, where they are again reflected, as in the inviscid case, see Fig. 2 (bottom right). Note that in both cases the inviscid characteristic path is closed and that the boundary layer thickness has the classical Ekman number dependency $O(E^{1/2})$.

When $\omega_0=0.74$, the velocity profiles inside the jet are similar to those studied analytically by Tilgner[15] in an unbounded domain. The longitudinal component, V_l, of fluid velocity in the direction of the jet (more precisely, in the direction of inviscid group velocity from the cylinder corner), is shown in Fig. 3 (top) at time $t=-T/8$ (where T denotes the piston period) and is perhaps best described as a jet profile. At $t=+T/8$, the profile of V_l in Fig. 3 (bottom) is that of a shear layer. We recall that $t=0$ refers to the time where the instantaneous cylinder height h is maximal and hence the piston velocity is zero. The source of the jets is the oscillating volume flux from the piston corners coming from the sidewall Stokes layer [which is much stronger than the (secondary-flow) boundary layer on the piston face and thus dominates the volume flux from the corner ring source]. Classical Stokes-layer theory gives a volume flux with a phase lag of $\pi/4$ relative to piston velocity, corresponding to a time delay of $T/8$. Thus, the volume flux should be zero (the "shear-layer" profile for V_l) when $t=+T/8$ and maximal (the jet profile for V_l) when $t=-T/8$, in accord with the results of Fig. 3. This is seen in our simulation, which shows (Fig. 3) similar profiles for the azimuthal (V_θ) and longitudinal (V_l) velocity components at times a quarter of a piston cycle ($T/4$) apart. The velocity profiles are different from Tilgner's results away from the jet region because of the presence of the walls.

The jet width is defined (before the first wall reflection) as the distance between the two transverse points where the squared velocity is one half its maximum. Figure 4 shows the E dependency of the jet width. The scaling $O(E^{1/3})$ is found in the case $\omega_0=0.74$, as in Tilgner's unbounded analysis, whereas when $\omega_0=0.4472$, the exponent is closer to $1/4$. The difference between the two cases is that, as we saw earlier, when $\omega_0=0.4472$, the inertial wave packet undergoes multiple reflections, leading to many superimposed jets in the form of a cross. If the phase of these jets is such that they mutually reinforce, their combined effect is of width $O(E^{1/4})$. This is because, as shown by Tilgner, a jet having propagated a distance R has width $O(E^{1/3}R^{1/3})$, growing with propagation distance due to viscous diffusion. Viscous effects in the boundary layer also cause attenuation at each reflection, which limits the propagation distance to be $R_{\max}\sim E^{-1/4}$ or less. Superposition of the many jets with this order of propagation distance yields a final jet width of order $E^{1/3}R_{\max}^{1/3}\sim E^{1/4}$.

It is interesting to note that Stewartson's results for the steady split-disk problem,[17] which shows both $E^{1/3}$ and $E^{1/4}$ layers, can also be interpreted in the above fashion. Thus, if the integrand in Stewartson's Eq. (4.4) is re-expressed as an infinite sum of exponentials, each term in the sum can be interpreted as a reflected jet of Tilgner's type. These results

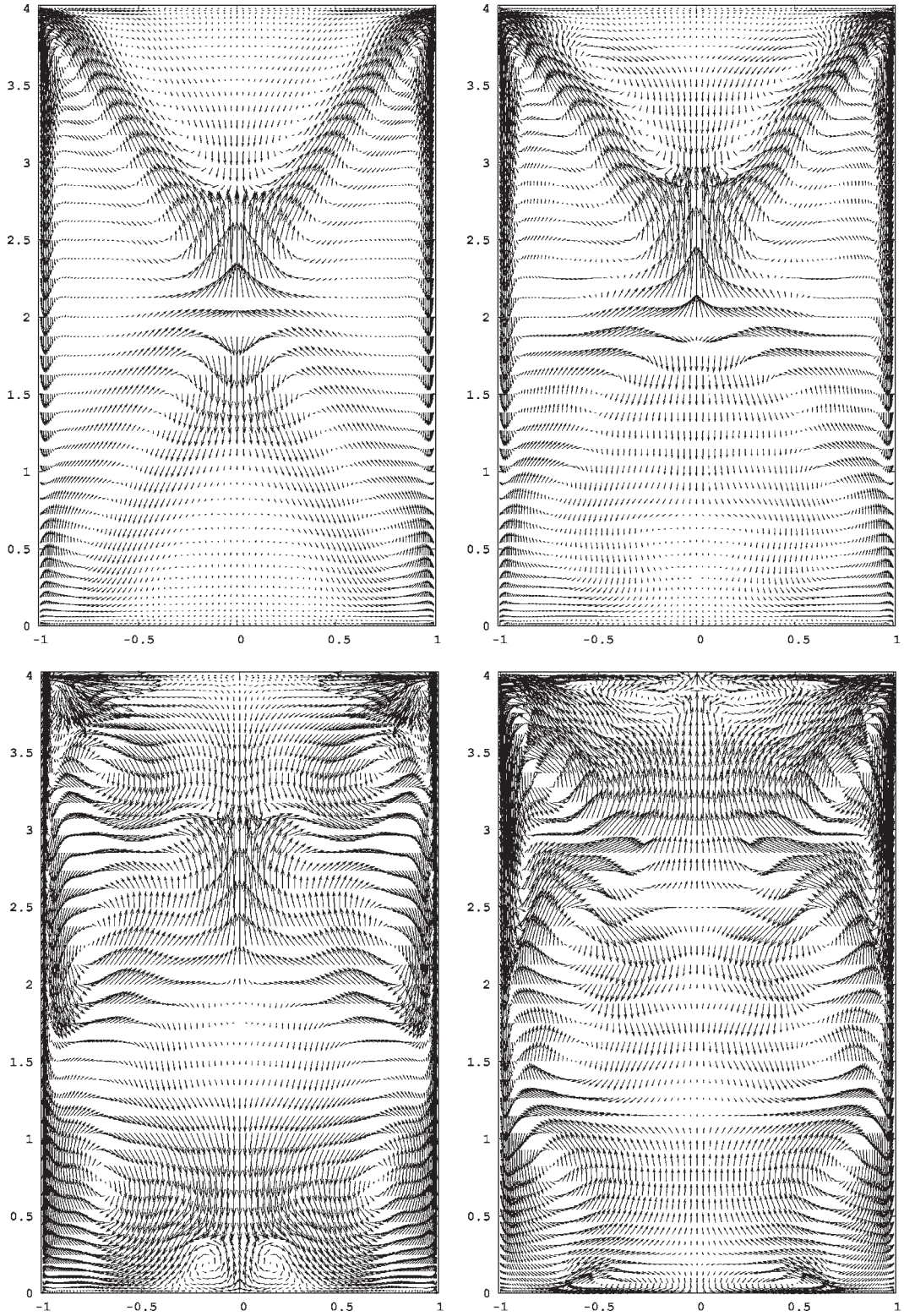

FIG. 5. Velocity field $\boldsymbol{V}$ in a plane through the cylinder axis ($E=2\times10^{-4}, \omega_0=0.4472$) for increasing values of $\epsilon=5.1\times10^{-3}$ (top left), $\epsilon=8.84\times10^{-2}$ (top right), $\epsilon=0.2$ (bottom left), and $\epsilon=0.3$ (bottom right). The velocity scale is reduced from plot to plot.

show that structures of width $O(E^{1/4})$ are to be expected in rotating flows when multiple reinforcing reflections occur.

B. Larger forcing amplitudes

We focus now on the effect of larger forcing amplitudes and proceed by letting the code run for $E=2\times10^{-4}$, $h_0=4$, and $\omega_0=0.4472$, increasing the value of ϵ every fiftieth piston cycle from $\epsilon=10^{-3}$ (where the dynamics are essentially linear) up to $\epsilon=0.3$ (see Fig. 5, which illustrates the following discussion). For small enough ϵ, the dynamics are linear, the spectrum is dominated by the fundamental piston frequency, as shown in Fig. 6 (bottom), and the structure of the

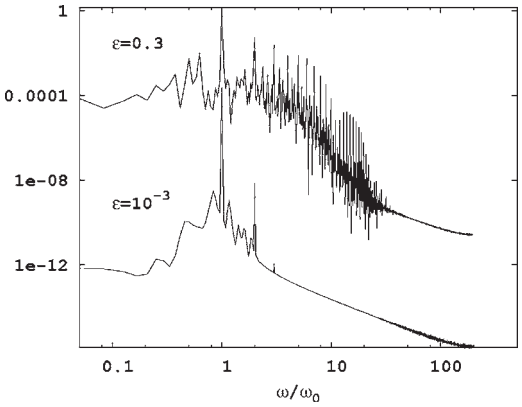

FIG. 6. Frequency spectrum of radial velocity at the spatial point $r=0.094$, $Z=h_0/2$ for $E=10^{-4}$, $\omega_0=0.4472$ and $\epsilon=10^{-3}$ (bottom), $\epsilon=0.3$ (top).

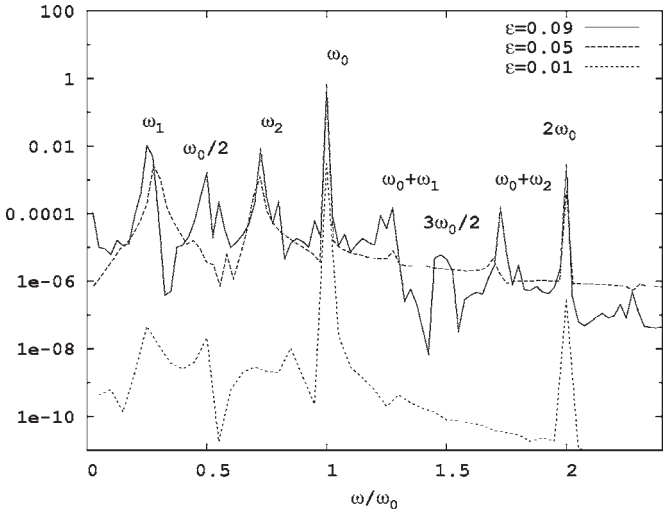

FIG. 7. Axial velocity spectrum at the spatial point $r=0.094$, $Z=h_0/2$ for $E=10^{-4}$, $\omega_0=0.775$ and $\epsilon=0.01$ (bottom), $\epsilon=0.05$ (middle), $\epsilon=0.09$ (top).

flow is as in Fig. 2 (top left). For ϵ between 0.02 and 0.06, the flow field is slightly modified, the most striking feature being the tendency of the jet to meander. For ϵ between 0.06 and 0.13, the cross pattern is more distorted and is visible only when $h(t)$ is near its maximum or minimum. A strong toroidal vortex is observed to develop near the upper corner and oscillates in phase with the piston. Finally, for $\epsilon>0.19$, the jet structure completely disappears, and it is no longer easy to distinguish any structures oriented at the theoretical angle $\phi=\arcsin\omega_0$. The flow then consists of a relatively complicated system of vortices induced by ejection and diffusion of vorticity generated at the upper corner. The velocity spectrum (see top of Fig. 6) now contains harmonics, but the flow remains periodic and is still dominated by the ω_0 angular frequency. The azimuthal component of the flow is found to develop a significantly nonzero mean when $\epsilon\geqslant 0.2$. This nonlinear effect is reminiscent of the precursor for breakdown in McEwan's experiment. Whether the assumption of axisymmetry is still valid for such large values of ϵ would need to be checked experimentally or using a 3D code and this is left for a future study.

IV. INSTABILITY OF THE FLOW

In the case $\omega_0=0.4472$ of Sec. III B, increasing ϵ always leads to an ω_0 periodic flow, despite the change in the spatial structure. Defining the basic flow as strictly ω_0 periodic, we have not so far seen any instability of this flow. In this section, we show that another forcing frequency, $\omega_0=0.775$, leads to richer dynamics. Following the strategy used in the previous section, we proceed by fixing $\omega_0=0.775$, $E=10^{-4}$, and progressively increasing the value of ϵ, starting from the linear regime.

A. Triadic instability

When ϵ is low enough, for example $\epsilon=0.01$, the frequency spectrum of the velocity components (see the lowest curve in Fig. 7) shows a strong peak at ω_0 and other weaker harmonics. This ω_0 periodic flow corresponds to the basic flow. As in earlier sections, the flow features conical jets emanating from the corners; these undergo two reflections on the side wall $r=1$ and form an open pattern. The jets cross at the axis when $Z\sim 3.2\pm 0.2$ (the uncertainty being due to the finite jet width) and are orientated at $51.3°\pm 5°$ with the rotation axis. This matches the inviscid theoretical angle $\arcsin\omega_0=50.8°$.

It is useful to adopt a modal description of the flow. The inviscid normal modes of the cylinder are described in the Appendix. They form an infinite discrete set, each mode having a characteristic natural frequency. The complex eigenfunctions of the modes yield a basis set, in terms of which a general solenoidal velocity field, in particular the numerically determined flow, can be expanded. The same is true of the viscous eigenmodes, whose characteristic (complex) frequencies and velocity eigenfunctions can be computed numerically.[22] Both inviscid and viscous modal descriptions are used in what follows. At small enough E, the viscous and inviscid modes differ significantly only in the boundary layers at the walls. The viscous eigenfrequencies are shown in Fig. 8 for $E=10^{-4}$. This figure represents the complex σ plane, where $\sigma=\tau+i\omega$ corresponds to the modal time dependence $e^{-\sigma t}$. Note that the modal damping factor $\tau=\Re(\sigma)$ is

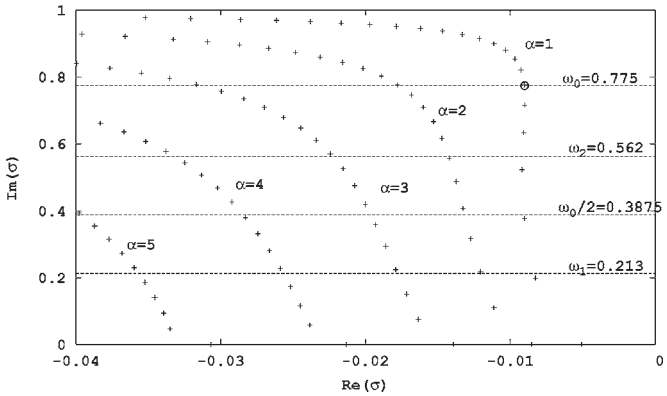

FIG. 8. Upper-half part of the complex eigenvalue spectrum of the linearized viscous operator in the absence of forcing, for $h_0=4$ and $E=10^{-4}$. Also shown are the isofrequencies $\omega=\omega_0$, $\omega=\omega_0/2$, $\omega=\omega_1$ and $\omega=\omega_2$ (see text for definitions of ω_1 and ω_2) and the isoradial wave number families. The mode (1,6) is indicated by a circle.

small compared to the frequency $\omega=\Im(\sigma)$; the modes are oscillatory and close to their inviscid counterparts. Nonetheless, modal damping is important because it limits the modal response at or near resonance. Note that the modal families corresponding to different values of the radial index α appear clearly in the figure [see the Appendix for the definition of the inviscid mode indices (α,m)].

For classical forced oscillators, direct resonance occurs if the natural frequency of the oscillator is close to the forcing frequency. Damping relaxes this notion of closeness and prevents the resonant amplitude from becoming infinite. In our case, inertial modes lying within $O(E^{1/2})$ of the horizontal line $\omega=\omega_0$ in Fig. 8 are likely to undergo direct resonance. In the present case, one low-order mode (indicated by a circle) has a natural frequency $\omega=0.7759$ very close to the chosen value of ω_0. Its spatial structure consists of a vertical row of six equally sized cells, each cell corresponding to a toroidal vortex, thus allowing identification of the viscous mode as corresponding to the inviscid mode (1,6). Such identification is used throughout to label viscous modes. Another relatively weakly damped mode lying in the vicinity of $\omega=\omega_0$ is (2,11).

For $\epsilon=0.05$, the frequency spectrum is still dominated by the ω_0 peak, but also displays other smaller peaks at angular frequencies $\omega_1=0.213$ and $\omega_2=0.562$. The flow is no longer strictly ω_0 periodic, indicating that the basic flow has undergone instability. It is striking that $\omega_1+\omega_2=\omega_0$. All other combinations of ω_1, ω_2 with ω_0 and its harmonics are also present in the spectrum, among them $\omega_0+\omega_1$, $\omega_0+\omega_2$, $2\omega_0+\omega_1$, $2\omega_0+\omega_2$, …. The modal eigenfrequency spectrum in Fig. 8 shows that many modal frequencies lie near the horizontal lines $\omega=\omega_1$ and $\omega=\omega_2$, some of these correspond to low-order modes, others to more strongly damped modes of higher order. The least damped modes of frequency $\omega\sim\omega_1$ are found to be (2,2), (3,3), (4,4), (5,4), (5,5), …. Those with frequency $\omega\sim\omega_2$ are (2,6), (3,8), (3,9), (4,12), (4,13), (5,14), ….

The velocity time-series at any spatial point may be Fourier-transformed, then filtered around the angular frequency ω_0 and brought back into the time domain by inverse Fourier transforming. Such a procedure will be referred to as "filtering the flow at frequency ω_0." In the present case, it yields a velocity field $\boldsymbol{V}|_{\omega_0}$, shown in Fig. 9, whose spatial structure is very reminiscent of the mode (1,6). Boundary layers are also apparent, as are, with a smaller but distinguishable amplitude, thin jets emanating from the piston corners.

A more quantitative measure of the relative importance of modal contributions to the flow than visual recognition from the velocity field is provided by the *modal energy factor*:[21]

$$b^{(\mu)}=\frac{2\left|\int \boldsymbol{u}\cdot\boldsymbol{u}^{(\mu)*}d^3\boldsymbol{X}\right|^2}{\int|\boldsymbol{u}|^2d^3\boldsymbol{X}}, \tag{1}$$

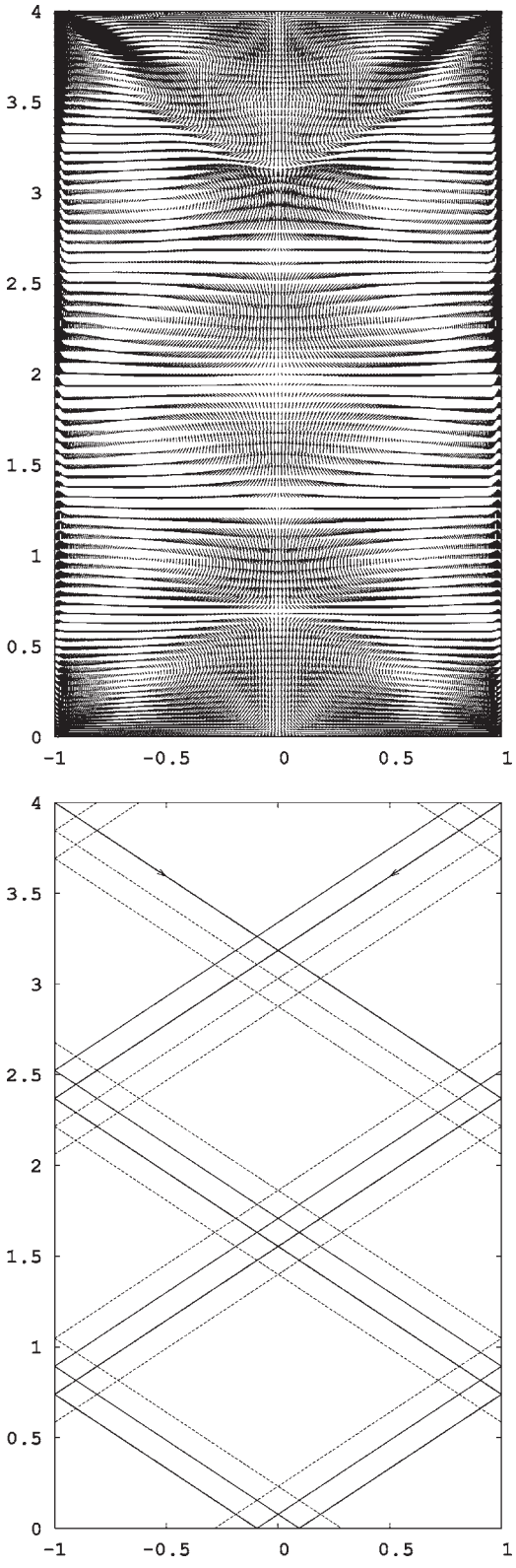

FIG. 9. Filtered velocity field $\boldsymbol{V}|_{\omega_0}$ in a plane through the cylinder axis ($\epsilon=0.05$, $E=10^{-4}$, $\omega_0=0.775$), visualized after 179.5 piston cycles. Comparison with the corresponding inviscid inertial cones.

where $\boldsymbol{u}^{(\mu)}$ is an inviscid mode and, in the present case, $\boldsymbol{u}=\boldsymbol{V}|_{\omega_0}$. The factor of 2 accounts for the complex conjugate mode, which is always present alongside (and is physically indistinguishable from) mode μ when a real velocity field is

expressed as a modal sum. We find $b^{(1,6)}=28.5\%\pm3.2\%$, where the $\pm3.2\%$ corresponds to time variations over a modal cycle. This means that the mode (1,6) accounts for around 28.5% of the energy of the ω_0 component of the flow. Computing $b^{(\mu)}$ for other modes gives much smaller values, indicating their lesser importance. For instance, the mode (2,11), also likely to be directly forced, represents only $0.82\%\pm0.07\%$ of the energy. Thus, the filtered flow $\boldsymbol{V}|_{\omega_0}$ consists of the resonant mode (1,6) and a large number of other modes which are much less energetic. This may be contrasted with the cases studied in earlier sections, for which calculation of the b's shows no single mode to energetically dominate the others.

The same process can be repeated for both the frequencies ω_1 and ω_2. The filtered flow $\boldsymbol{V}|_{\omega_1}$ (shown in Fig. 10) is a superposition of oscillating large-scale vortices (reflecting the presence of low-order inertial modes) and conical jets orientated at 14° to the rotation axis, not far from the theoretical angle $\arcsin\omega_1=12.3°$. However, whereas the ω_0 jets emanate from the piston corners, the ω_1 jets originate in a region located on the axis. More precisely, they emerge from the focal region of the ω_0 jets, where the basic flow has largest kinetic energy and hence where nonlinear effects are locally the strongest. Calculation of $b^{(\mu)}$ for $\boldsymbol{V}|_{\omega_1}$ and different modes shows that the mode (2,2) is the most important, representing $29\%\pm1\%$ of the energy. Other low-order modes make a smaller but still significant contribution to the energy of the filtered flow: among them, the most energetic are (3,3) ($b^{(3,3)}=10.4\%\pm0.4\%$), and (4,4) ($b^{(4,4)}=2.7\%\pm0.3\%$). Not surprisingly, these three modes have viscous angular frequencies 0.2166, 0.2238, and 0.2278, close to $\omega=\omega_1$ in Fig. 8.

The flow $\boldsymbol{V}|_{\omega_2}$ also contains low-order inertial modes, superimposed on cone-like jets, inclined at 38° ($\arcsin\omega_2=34.2°$), which emanate from the same region as the ω_1 jets. Calculation of b's shows that the mode (3,8) has the highest energetic contribution to the flow $\boldsymbol{V}|_{\omega_2}$, representing $25\%\pm1.25\%$. Other energetically important modes yield $b^{(2,8)}=1.35\%\pm0.27\%$, $b^{(4,9)}=3\%\pm0.3\%$, $b^{(4,11)}=1.2\%\pm0.2\%$, $b^{(4,12)}=2.1\%\pm0.15\%$, $b^{(4,13)}=1.135\%\pm0.1\%$, and $b^{(5,14)}=1.6\%\pm0.3\%$. Most of these also correspond to points located near the line $\omega=\omega_2$ in Fig. 8.

It appears from the above discussions, that the peaks at ω_0, ω_1 and ω_2 can be interpreted as modes oscillating close to their natural frequencies. Recalling that $\omega_1+\omega_2=\omega_0$, this indicates the existence of modal triads whose frequencies satisfy such a resonance condition. However, not all modes located near the lines $\omega=\omega_1,\omega_2$ in Fig. 8 are present in our computation, e.g., modes such as (1,1), (3,9), …. This suggests that additional constraints on possible triads, over and above the condition on frequencies, need to be fulfilled. The most energetic modes at each frequency ω_0, ω_1, and ω_2 are $\mu_0=(1,6)$, $\mu_1=(2,2)$, and $\mu_2=(3,8)$, and are seen to satisfy the modal-index conditions $m_2-m_1=m_0$, $\alpha_2-\alpha_1=\alpha_0$ (as well as $n_2-n_1=n_0$, since $n_0=n_1=n_2=0$ by axisymmetry).

B. Subharmonic instability

For $\epsilon=0.09$, the frequency spectrum is similar to the case $\epsilon=0.05$ except that it contains an additional peak at angular frequency $\omega=\omega_0/2$. Such subharmonic response of the system at half the piston frequency, as well as the existence of an ϵ threshold for this peak are both reminiscent of the parametric instability observed in the case $\omega_0>1$.[21] Calculation of the $b^{(\mu)}$ for the filtered flows $\boldsymbol{V}|_{\omega_0}$, $\boldsymbol{V}|_{\omega_1}$, and $\boldsymbol{V}|_{\omega_2}$ returns values close to those from the previous case $\epsilon=0.05$ and the qualitative structure of these flows is similar (see Fig. 9). Calculation of the $b^{(\mu)}$'s for the flow $\boldsymbol{V}|_{\omega_0/2}$ indicates that energy is mostly contained in the mode (2,4) ($b^{(2,4)}=35.8\%\pm0.7\%$). The modes (1,2) ($b^{(1,2)}=3.15\%\pm0.11\%$) and (4,8) ($b^{(4.8)}\sim1.1\%$) are also noticeable. These modes have eigenfrequencies close to $\omega=\omega_0/2$ (see Fig. 8). The velocity field $\boldsymbol{V}|_{\omega_0/2}$ (shown in Fig. 10, top right) consists principally of the mode (2,4) and a high-speed zone near the axis. It is harder than in the cases ω_0, ω_1, and ω_2 to distinguish a jet-like structure from either the corner or the axis.

C. Discussion

Following the analysis of Racz,[20] any perturbation $\boldsymbol{u}(\boldsymbol{X},t)$ of the basic flow $\boldsymbol{V}=\boldsymbol{U}(\boldsymbol{X},t)$ can be expanded using the orthogonal basis of inviscid inertial modes as

$$\boldsymbol{u}=\sum_{\mu}B_{\mu}(t)\boldsymbol{u}^{(\mu)}(\boldsymbol{X}) \tag{2}$$

where, in our case, the sum is over all axisymmetric modes. Assuming small ϵ, small $E=O(\epsilon^2)$, and expressing the viscous damping terms using boundary layer analysis, yields a dynamical system for the modal amplitudes $B_{\mu}(t)$:

$$\frac{dB_{\mu}}{dt}+i\omega^{(\mu)}B_{\mu}=\underbrace{-2\epsilon\frac{d}{dt}\left(\sum_{\nu}C_{\mu\nu}B_{\nu}\cos\omega_0 t\right)}_{\text{Coupling by piston motion}}\underbrace{-E^{1/2}\zeta_{\mu}B_{\mu}}_{\text{Viscous damping}}+\underbrace{i\sum_{\nu_1,\nu_2}\Lambda_{\mu\nu_1\nu_2}B_{\nu_1}B_{\nu_2}}_{\text{Nonlinearity}}$$

$$+\underbrace{\sum_{\nu}B_{\nu}\int(\boldsymbol{U}\cdot(\boldsymbol{u}^{(\nu)}\cdot\nabla)+\boldsymbol{u}^{(\nu)}\cdot(\boldsymbol{U}\cdot\nabla))\boldsymbol{u}^{(\mu)^*}d^3\boldsymbol{X}}_{\text{Interaction with the basic flow}}. \tag{3}$$

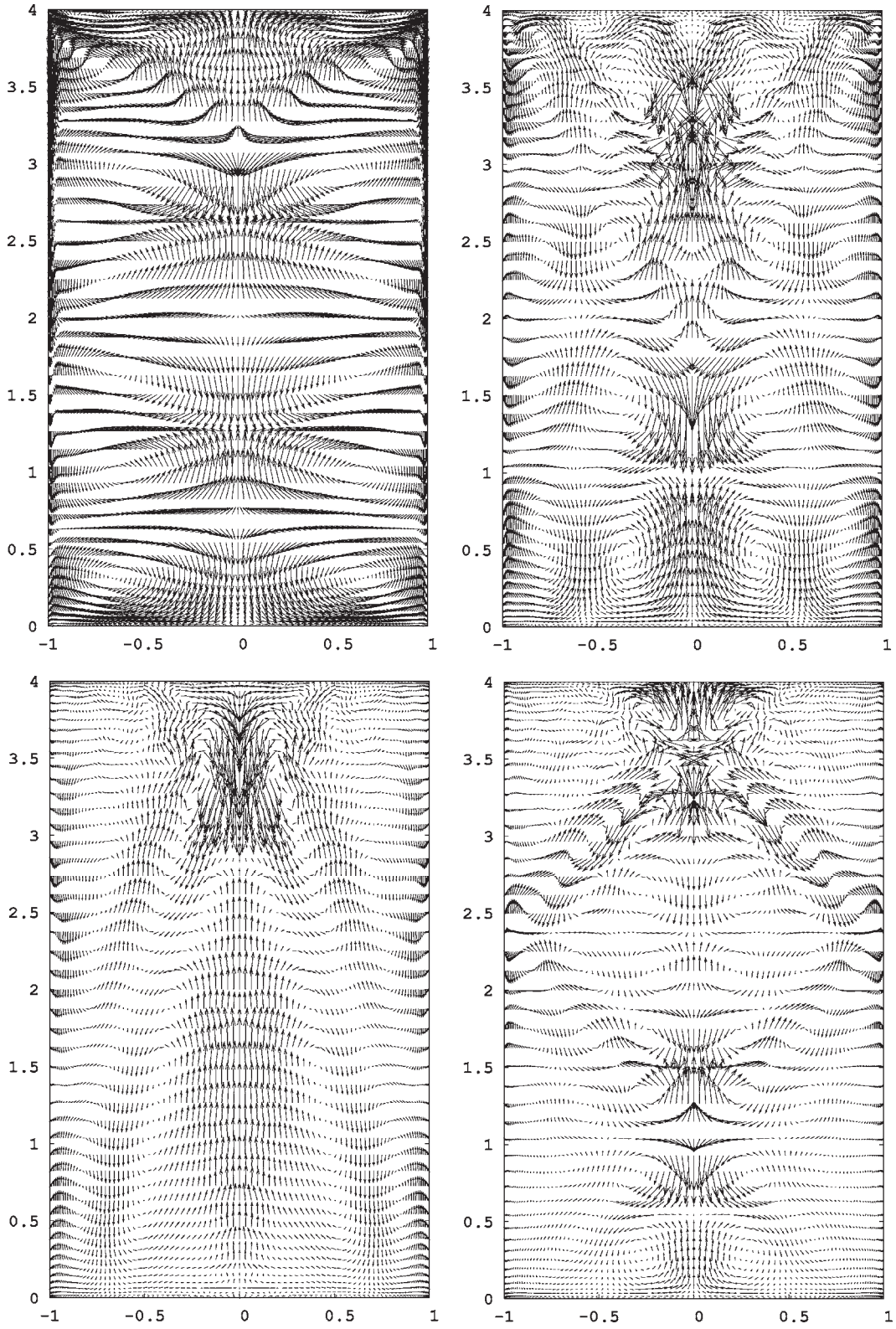

FIG. 10. Filtered velocity field $\boldsymbol{V}|_\omega$ in a plane through the cylinder axis ($\epsilon=0.09$, $E=10^{-4}$, $\omega_0=0.775$). Each plot shows a different filtered component $\boldsymbol{V}|_\omega$, visualized after 79 piston cycles: $\omega=\omega_0$ (top left), $\omega=\omega_0/2$ (top right, velocity scale multiplied by 9), $\omega=\omega_1$ (bottom left, velocity scale multiplied by 3), $\omega=\omega_2$ (bottom right, velocity scale multiplied by 3).

In this equation, all terms on the right-hand side are asymptotically small and $B_\mu=\epsilon^{1/2}A_\mu e^{-i\omega^{(\mu)}t}$ at leading order, where A_μ is a slowly varying amplitude. Evolution equation for the A_μ's arise at higher order from nonsecularity conditions involving terms on the right-hand side whose fast-time frequency is sufficiently close ($O(\epsilon)$) to the natural frequency, $\omega^{(\mu)}$. In Racz,[20] it was supposed that direct resonance of a mode did not occur and consequently that $\boldsymbol{U}=o(\epsilon)$ outside

the boundary layers. In that case, the final term in Eq. (3) is asymptotically negligible. However, as we shall see, this is not always the case.

The remaining terms on the right-hand side of Eq. (3) were allowed for in Racz's analysis. The first represents modal coupling by piston motion and is resonant if

$$|\omega^{(\mu)} - \omega^{(\nu)}| = \omega_0 + O(\epsilon) \tag{4}$$

and if the coupling coefficient $C_{\mu\nu} \neq 0$. For axisymmetric modes which concern us here, $C_{\mu\nu}=0$ unless the modes μ and ν are complex conjugates. Since, in that case, $\omega^{(\mu)} = -\omega^{(\nu)}$, resonant coupling, and hence instability via this mechanism, can only occur if $|\omega^{(\mu)}| = \omega_0/2 + O(\epsilon)$. The result, provided the piston amplitude exceeds a certain viscous threshold, is a subharmonic instability with slow-time growth of the modal pair (μ, ν). One can interpret this instability as resulting from a resonant triadic interaction between the unstable mode pair and the axial piston motion. This instability has also been studied numerically[21] and experimentally.[23]

The second term on the right-hand side of Eq. (3) represents viscous damping which tends to resist the instability, leading to the piston amplitude threshold referred to above. The nonlinear term involves the interaction matrix

$$\Lambda_{\mu\nu_1\nu_2} = -\frac{i}{2}\int (u_i^{(\nu_1)} u_j^{(\nu_2)} + u_i^{(\nu_2)} u_j^{(\nu_1)}) \frac{\partial u_i^{(\mu)^*}}{\partial X_j} d^3\boldsymbol{X} \tag{5}$$

which is nonzero if $m_\mu = \pm m_{\nu_1} \pm m_{\nu_2}$ and $n_\mu = n_{\nu_1} + n_{\nu_2}$, where m and n are axial and azimuthal modal orders. Note that the condition on n is automatically satisfied for axisymmetric modes.

When there is direct resonance of a low-order mode μ_0, i.e., $\omega^{(\mu_0)} = \omega_0 + O(\epsilon)$, the basic flow $\boldsymbol{U}$ becomes $O(\epsilon)$ throughout the cylinder and the final term in Eq. (3) is no longer negligible. In that case, $\boldsymbol{U}$ is dominated by mode μ_0 and $\boldsymbol{U} \sim \Re(A_0 e^{-i\omega_0 t}\boldsymbol{u}^{(\mu_0)})$. Introducing this expression into the integral in Eq. (3), the final term can be written in terms of $\Lambda_{\mu\mu_0\nu}$ and $\Lambda_{\mu\bar{\mu}_0\nu}$, where the overbar denotes modal conjugation. The corresponding resonance conditions are Eq. (4) and $m_\mu = \pm m_\nu \pm m_{\mu_0}$ (plus a condition on n_μ, $n_{\mu 0}$ and n_ν in the nonaxisymmetric case). This can lead to an instability involving growth of the mode pair (μ, ν) due to interactions of the modal triad μ, ν, μ_0, provided that $|A_0|$ exceeds a certain viscous threshold. Kerswell[24] studied the similar case of triadic instabilities arising from saturation of a primary instability. Note that, compared with the subharmonic instability studied by Racz, which originates from the first term in Eq. (3), there is no requirement for the modes μ and ν to be conjugates.

We turn next to the results of our numerical study discussed earlier in Secs. IV A and IV B. For $\epsilon=0.01$, the basic flow is stable and includes the directly resonant mode (1,6). For $\epsilon=0.05$, the appearance of two additional spectral peaks at ω_1 and ω_2, $\omega_1+\omega_2=\omega_0$, indicates an instability. The principal modes constituting the flow are then (1,6), (2,2), and (3,8), of which the latter two have natural frequencies close to ω_1 and ω_2. Interpreting the modes as $\mu_0=(1,6)$, $\mu=(2,2)$, and $\nu=(3,8)$, μ_0 is indeed directly resonant while μ and ν satisfy the conditions (4) and $m_\mu = \pm m_\nu \pm m_{\mu_0}$, necessary for the triadic instability described above. Note that (1,6) is always directly resonant, and hence is present even at small ϵ, whereas (2,2) and (3,8) require that ϵ exceed a certain viscous threshold.

When $\epsilon=0.09$, a subharmonic peak at $\omega_0/2$ appears in addition to the triadic frequencies ω_1 and ω_2. This suggests the presence of a subharmonic instability arising from parametric resonance of conjugate axisymmetric modes with the piston motion of the type discussed earlier. The two modes (1,2) and (2,4), which were previously identified in the flow, have inviscid natural frequencies of, respectively, 0.3793 and 0.408. The former is very close to $\omega_0/2=0.3875$, while the latter, though close, is less well tuned. Either mode could induce subharmonic instability and the calculated piston amplitude thresholds (obtained from $\epsilon_c = \tau/\omega C$) are $\epsilon_c^{(1,2)} = 0.0557$ and $\epsilon_c^{(2,4)} = 0.07819$. These threshold values are consistent with the appearance of both modes in the flow for $\epsilon = 0.09$ and their absence for $\epsilon=0.05$. This being said, it is perhaps surprising that the mode (2,4), which has a higher instability threshold and is further in natural frequency from $\omega_0/2$, is more energetic than (1,2). Note that nonlinear and viscous effects modify the modal frequencies and can either tune or detune a given mode with respect to parametric resonance. A similar situation was found by Mason and Kerswell[25] in a numerical simulation of the elliptical instability. In their study, two nonaxisymmetric mode pairs are in competition and the less well-tuned one is found to have a larger growth rate.

The dynamics of the modes (1,2) and (2,4) is complicated by the existence of a resonant triad with the mode (1,6). Thus, taking $\mu_0=(1,6)$, $\mu=(1,2)$ and $\nu=\overline{(2,4)}$, the conditions for triadic resonance are satisfied. Whereas in Duguet *et al.*[21] the essential modal dynamics involved only a single primary mode (as well as geostrophic secondary ones), here there are two competing candidates for subharmonic resonance, (1,2) and (2,4), triadically coupled to a directly resonant mode, (1,6), itself forming part of a second triad with (2,2) and (3,8).

V. CONCLUSION

We have shown that a rotating flow subject to axial periodic strain of frequency $\omega_0 < 1$ can exhibit much richer dynamics than the case $\omega_0 > 1$ studied earlier. The flow has been investigated numerically using an axisymmetric spectral code. For small enough piston amplitude ϵ, it is found to be periodic with the forcing frequency, but for larger amplitudes, this periodic basic flow can become unstable and aperiodic behavior is then found. When it is stable and ϵ is not too large, the basic flow shows thin oscillatory jets of conical shape, which are angled at arcsin ω_0 with the rotation axis. For nonvanishing E, these jets undergo a finite number of reflections at the walls. Their width scales like $O(E^{1/3})$ or $O(E^{1/4})$ when ω_0 is such that they retrace themselves after reflection. Increasing the value of ϵ leads to distortion and then disappearance of the jets due to nonlinear effects.

For certain resonant values of ω_0, direct forcing of a low-order inertial mode occurs. Such a mode can be triadi-

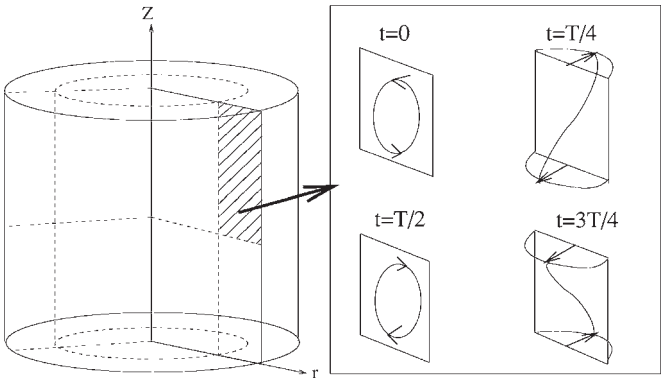

FIG. 11. Dynamics of a single cell for the inviscid inertial mode (2,2).

cally coupled with other inertial modes and generate new frequencies ω_1 and ω_2, $\omega_1+\omega_2=\omega_0$, provided that the piston amplitude exceeds a certain viscous threshold. New jets appear in the flow, with an inclination corresponding to the resonant frequencies of the triad. Instability can also occur when there is resonance between two conjugate axisymmetric modes and the piston motion, which leads to subharmonic modal growth at half the forcing frequency. It is interesting to note that these instabilities provide a route towards quasiperiodicity in a flow which is purely axisymmetric. Experimental or 3D numerical investigation is needed to confirm the possibility of such multiperiodic axisymmetric states.

APPENDIX: AXISYMMETRIC INERTIAL MODES

Here we define the inviscid axisymmetric inertial modes of a rotating cylinder,[1,2] which are time-harmonic solutions of the linearized equations of motion. The velocity of each mode has the form $\boldsymbol{u}(\boldsymbol{X})e^{-i\omega t}$ where

$$u_r(\boldsymbol{X}) = iN\omega k J_0'(kr)\cos\left(\frac{m\pi Z}{h_0}\right), \tag{A1}$$

$$u_\theta(\boldsymbol{X}) = NkJ_0'(kr)\cos\left(\frac{m\pi Z}{h_0}\right), \tag{A2}$$

$$u_Z(\boldsymbol{X}) = iN\frac{\omega k^2 h_0}{m\pi}J_0(kr)\sin\left(\frac{m\pi Z}{h_0}\right). \tag{A3}$$

Here, $m\geqslant 0$ is an integer, J_0 is the usual zeroth order Bessel function, N is a normalization constant such that the mode has a unit L^2 norm and the angular frequency ω can be obtained from

$$\omega = \pm\left(1+\left(\frac{kh_0}{m\pi}\right)^2\right)^{-1/2}. \tag{A4}$$

The transverse wave number k is one of the positive roots of J_0', thus a given axisymmetric mode can be indexed by m, and k. The modal eigenfunctions form an orthonormal basis set for the space of solenoidal, complex vector fields having zero normal velocity at the cylinder boundaries and the L^2 complex inner product. The axisymmetric, nongeostrophic ($m\neq 0$) modes used in this paper can be indexed by the pair of integers (α,m), where the index $\alpha\geqslant 1$ represents the positive roots of $J_0'(k)=0$ in increasing order. Each mode consists of an array of αm oscillatory toroidal vortices, which, when viewed in a plane through the cylinder axis, appears as an array of rectangular cells [see Fig. 11, which shows the mode (2,2)]. There are α cells in the radial direction and m in the axial one. The cell heights are all the same, whereas the radial dimension varies. In addition to the velocity components u_r and u_Z which are represented in this plane, the azimuthal component u_θ oscillates in the phase quadrature.

[1] Lord Kelvin, "Vibrations of a columnar vortex," Philos. Mag. **10**, 155 (1880).
[2] H. P. Greenspan, *The Theory of Rotating Fluids* (Cambridge University Press, Cambridge, 1969).
[3] A. D. McEwan, "Inertial oscillations in a rotating cylinder," J. Fluid Mech. **40**, 603 (1970).
[4] R. Manasseh, "Breakdown regimes of inertia waves in a precessing cylinder," J. Fluid Mech. **243**, 261 (1992).
[5] J. J. Kobine, "Inertial wave dynamics in a rotating and precessing cylinder," J. Fluid Mech. **303**, 233 (1995).
[6] C. Eloy, P. Le Gal, and S. Le Dizès, "Elliptic and triangular instabilities in rotating cylinders," J. Fluid Mech. **476**, 357 (2003).
[7] L. Graftieaux, L. Le Penven, J. F. Scott, and N. Grosjean, "A new parametric instability in rotating cylinder flow," in Advances in Turbulence IX, Proceedings of the 9th European Turbulence Conference, Southampton, UK, 2–5 July 2002.
[8] R. R. Kerswell, "Elliptical instability," Annu. Rev. Fluid Mech. **34**, 83 (2002).
[9] J. Noir, D. Brito, K. Aldridge, and P. Cardin, "Experimental evidence of inertial waves in a precessing spheroidal cavity," Geophys. Res. Lett. **28**, 3785 (2001).
[10] L. Lacaze, P. Le Gal, and S. Le Dizès, "Elliptical instability in a rotating spheroid," J. Fluid Mech. **505**, 1 (2004).
[11] R. Hollerbach and R. R. Kerswell, "Oscillatory internal shear layers in rotating and precessing flows," J. Fluid Mech. **298**, 327 (1995).
[12] M. Rieutord and L. Valdettaro, "Inertial waves in a rotating spherical shell," J. Fluid Mech. **341**, 77 (1997).
[13] A. Tilgner, "Driven inertial oscillations in spherical shell," Phys. Rev. E **59**, 1789 (1999).
[14] W. W. Wood, "An oscillatory disturbance of rigidly rotating fluid," Proc. R. Soc. London, Ser. A **293**, 181 (1966).
[15] A. Tilgner, "Oscillatory shear layers in source driven flows in an unbounded rotating fluid," Phys. Fluids **12**, 1101 (2000).
[16] R. R. Kerswell, "On the internal shear layers spawned by the critical regions in oscillatory Ekman boundary layers," J. Fluid Mech. **298**, 311 (1995).
[17] K. Stewartson, "On almost rigid rotations, part 1," J. Fluid Mech. **3**, 17 (1957).
[18] F. Busse, "Shear flow instabilities in rotating systems," J. Fluid Mech. **335**, 77 (1968).
[19] R. Hollerbach, "Instability of the Stewartson layer, part 1," J. Fluid Mech. **492**, 289 (2003).
[20] J. P. Racz, "Instabilité paramétrique d'un cylindre de fluide en rotation soumis à une compression sinusoïdale périodique," Ph.D. thesis, Ecole Centrale de Lyon (2003).
[21] Y. Duguet, J. F. Scott, L. Le Penven, "Instability inside a rotating gas cylinder subject to axial periodic strain," Phys. Fluids **17**, 114103 (2005).
[22] Y. Duguet, "Simulation numérique de l'instabilité hydrodynamique dans un cylindre de gaz tournant soumis à une compression périodique," Ph.D. thesis, Ecole Centrale de Lyon (2004).
[23] L. Graftieaux, "Etude expérimentale de l'instabilité d'un cylindre tournant soumis à une compression périodique," Ph.D. thesis, Ecole Centrale de Lyon (2003).
[24] R. R. Kerswell, "Secondary instabilities in rapidly rotating fluids: inertial wave breakdown," J. Fluid Mech. **382**, 283 (1999).
[25] D. M. Mason and R. R. Kerswell, "Nonlinear evolution of the elliptical instability: an example of inertial wave breakdown," J. Fluid Mech. **396**, 73 (1999).